



On the trade-off between mode volume and quality factor in dielectric nanocavities optimized for Purcell enhancement

Işiklar, Göktug; Kristensen, Philip Trøst; Mørk, Jesper; Sigmund, Ole; Christiansen, Rasmus Ellebæk

Published in:
Optics Express

Link to article, DOI:
[10.1364/OE.474686](https://doi.org/10.1364/OE.474686)

Publication date:
2022

Document Version
Publisher's PDF, also known as Version of record

[Link back to DTU Orbit](#)

Citation (APA):
Işiklar, G., Kristensen, P. T., Mørk, J., Sigmund, O., & Christiansen, R. E. (2022). On the trade-off between mode volume and quality factor in dielectric nanocavities optimized for Purcell enhancement. *Optics Express*, 30(26), 47304-47314. <https://doi.org/10.1364/OE.474686>

General rights


Copyright and moral rights for the publications made accessible in the public portal are retained by the authors and/or other copyright owners and it is a condition of accessing publications that users recognise and abide by the legal requirements associated with these rights.

- Users may download and print one copy of any publication from the public portal for the purpose of private study or research.
- You may not further distribute the material or use it for any profit-making activity or commercial gain
- You may freely distribute the URL identifying the publication in the public portal

If you believe that this document breaches copyright please contact us providing details, and we will remove access to the work immediately and investigate your claim.



On the trade-off between mode volume and quality factor in dielectric nanocavities optimized for Purcell enhancement

GÖKTUĞ IŞIKLAR,^{1,2,*}  PHILIP TRØST KRISTENSEN,^{2,3}  JESPER MØRK,^{2,3} OLE SIGMUND,^{1,2} AND RASMUS ELLEBÆK CHRISTIANSEN^{1,2} 

¹Department of Civil and Mechanical Engineering, Technical University of Denmark, Nils Koppels Allé Building 404, 2800 Kongens Lyngby, Denmark

²NanoPhoton - Center for Nanophotonics, Technical University of Denmark, Ørstedes Plads 345A, 2800 Kongens Lyngby, Denmark

³Department of Electrical and Photonics Engineering, Technical University of Denmark, Ørstedes Plads 343, 2800 Kongens Lyngby, Denmark

*gokisi@dtu.dk

Abstract: This study explores the effect of geometric limitations on the achievable Purcell factor for single emitters in dielectric structures by employing topology optimization as an inverse design tool to maximize the local density of states. Nanobeams of different lengths with varying fixed central bridge widths are considered to investigate the impact of footprint and geometric length-scale. In single-mode photonic cavities, the Purcell factor is known to be proportional to the ratio of the quality factor Q to the effective mode volume V . Analysis of the optimized nanocavities shows a trade-off between quality factor and mode volume as a function of geometric limitations. Crucially, the design exhibiting the largest Purcell enhancement does not have the highest Q nor the lowest V found in the design pool. On the contrary, it is found that Q consistently drops along with decreasing V as the minimum allowed geometric length-scale decreases while the Purcell factor increases. Finally, the study provides insight into the importance of Q and V for enhancing the Purcell factor under geometric limitations.

© 2022 Optica Publishing Group under the terms of the [Optica Open Access Publishing Agreement](#)

1. Introduction

The spontaneous radiative decay rate of an emitter depends on its surroundings, and can be dramatically changed in microstructured geometries such as optical cavities [1]. The factor by which the rate is changed compared to an emitter in a vacuum is now known as the Purcell factor, and the effect has been experimentally demonstrated in different systems [2–5]. The Purcell effect finds practical applications in realizing efficient single-photon sources for quantum technology [6] as well as microscopic lasers and light-emitting diodes [7–10] among others. Due to fundamental interests and important applications, the design of cavities with large Purcell factors and small footprints continues to be of interest. In this work, we contribute to the field by identifying optimized designs under different experimentally relevant constraints.

In the situation where the linewidth of an emitter is smaller than the linewidth of the electromagnetic mode it couples to, the Purcell factor scales as Q/V , where Q is quality factor, and V is mode volume. Metallic structures, supporting plasmons with very small mode volumes but limited Q , have been experimentally demonstrated to result in very high Purcell factors. However, plasmonic structures are inherently lossy [11] and suffer from a limited quantum efficiency. Therefore, there is a strong interest in realizing high Purcell enhancement in dielectric structures, such as silicon or III-V semiconductors, where the material losses can be negligible. The possibility of achieving strong light-matter interactions with low-loss dielectric structures can

lead to integrating photonics and electronics for energy-efficient communication systems. Inverse design tools, which have been used for targeting unique light manipulation properties [12–14], can be utilized in searching for such extreme dielectric confinement structures. Specifically, topology optimization [15,16] is a robust inverse design tool for maximizing the Purcell factor [17] for a single emitter and hence used in this study. We note that optimization of the Purcell factor does not guarantee a single-mode cavity. In practice, however, we find that the structures are indeed single-mode near the target frequency; the gain in Purcell factor from the Q/V scaling appears to be the best way of optimizing the Purcell factor in all the cases considered. Also, since the structures are optimized to maximize the Purcell factor, there is no direct maximization (minimization) of Q (V) individually. Therefore, the optimized designs might favor improving one metric to the other for finding the largest possible Purcell factor. In other words, it might be the case that optimized nanobeam cavities with comparable Purcell factors can be realized through different combinations of Q and V under different geometric limitations. Understanding this interplay between Q and V will provide insight into the physics and limits of the problem and create room for exploring and tailoring the optimized nanocavities.

The interest in nanobeam cavities is growing due to their ability to significantly enhance the rate of different optical processes while having relatively small footprints and being relatively easy to integrate with other nanophotonic devices [20,21]. Thanks to their practical advantages, we focus on dielectric nanobeam cavities in the present work (a simplified design is sketched in Fig. 1). Over the past decades, increasing Q and decreasing V have been targeted in multiple previous works [17–25] in order to improve the Purcell factor. Experimentally measured Q values exceeding 11×10^6 (recorded from one of the nine cavities with around $8.65 \mu\text{m} \times 3.2 \mu\text{m}$ dimensions that are positioned on a $300 \mu\text{m} \times 15 \mu\text{m}$ area) have been achieved by Asano et al. [23], using large scale planar photonic crystal cavities. The magnitude of the achievable temporal confinement is highly affected by the size of the nanocavity [26,27]. Therefore achieving high Q values is challenging for small cavities with footprints on the order of the wavelength. Meanwhile, for a wide range of practical applications such as on-chip photonic integration, downsizing of photonic devices is required, thus limiting the realizable Q values. In such cases, strong spatial confinement (low V) is required to achieve high Purcell enhancement. Obtaining V values even smaller than the so-called diffraction limit of $(\lambda/2n)^3$ (where λ is the wavelength and n is the refractive index of the medium in which the wave is confined) is a key to reaching the downscaling goal [28]. Furthermore, small mode volume cavities can be utilized in several applications such as optomechanical interaction [29], quantum indistinguishability [30], on-chip optical transduction [31], optical quantum computing [32], terahertz frequency synthesis [33]. To realize a low mode volume an air slotted nanobeam structure (similar to the nanobeam in Fig. 1(a) but with a continuous air slot) was introduced by Robinson et al. [18] which reduces V by exploiting the electric displacement boundary conditions at the solid/air interface in the slot. Later, Hu et al. [22] and Choi et al. [19] suggested designs with a dielectric bridge with a narrow width across the air slot region (Fig. 1(b)) to achieve even lower V values utilizing the same principle of discontinuous boundary conditions on the electric field. Note that the realizable mode volume relies on the bridge width (denoted with w_b in Fig. 1(b)) in such nanocavities. In their work, Choi et al. numerically demonstrated extremely low mode volume nanobeams with dielectric-mode (Fig. 1(c)) and air-mode confinement (Fig. 1(d)) with the help of the bowtie structures; and reported an air-mode confined V of $5.61 \times 10^{-4}(\lambda/2n_{\text{air}})^3$ for an air-slot width of 1 nm.

In the present work, we focus on the confinement of the optical field inside the dielectric, a challenge that has so far proven more difficult than air confinement. The mechanisms and challenges related to light concentration in air versus solid, as well as the influence of key geometrical parameters of bowtie structures, such as length-scale and the radius of curvature, are further discussed in Albrechtsen et al. [25]. The freedom to select the design domain size for

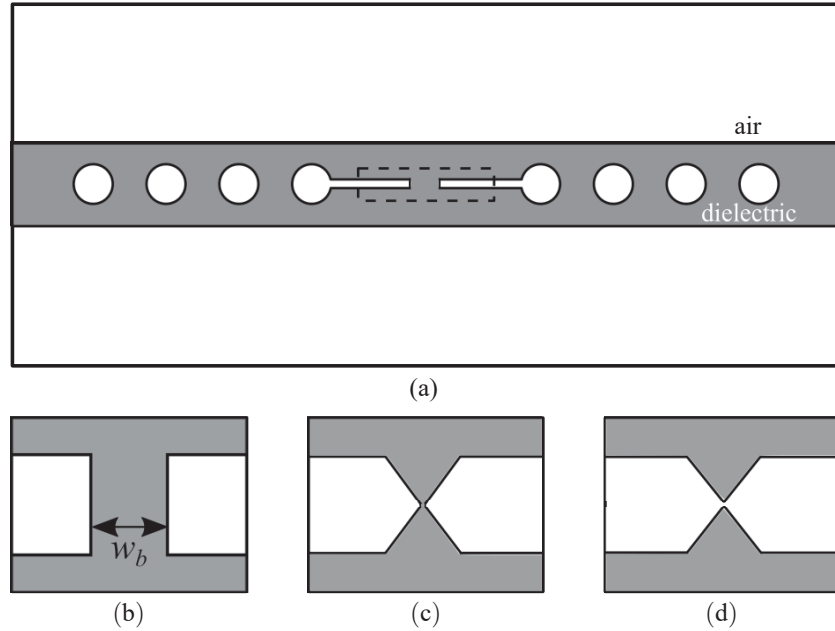


Fig. 1. (a) Representative visualization of a nanobeam cavity design with air slot and dielectric bridge (white and gray colored regions represent air and dielectric material, respectively) where the different version of slot structure is depicted with the zoomed-in images of the central part of the nanobeam: (b) slot-bridge structure where w_b denotes the bridge width, (c) dielectric-mode bowtie, (d) air-mode bowtie. The representative designs are adopted from Robinson et al. [18], and Choi et al. [19].

the nanobeam and the individual feature sizes (e.g., the bridge width) is practically constrained by the application-driven design-goal of reducing the footprint of optoelectronic devices and the minimum feature sizes imposed by fabrication, respectively. In this work, we impose these geometric limitations as fixed overall device size and fixed minimum bridge width. While this study is focused on two particular constraints, namely footprint and central feature size, a recent study [24] demonstrated that topologically optimized nanocavities can be fabricated using state-of-the-art methods by incorporating fabrication constraints in the design process. Further, it is possible to impose other fabrication constraints, such as achievable aspect ratio and minimum feature area, directly in the design process through additional geometric constraints [34]. A topology optimization problem is formed for analyzing the behavior of Q and V when designing nanocavities with high Purcell factors. To this end, we study various fixed-length silicon nanobeam cavities (1λ , 2λ , and 4λ design domains, where λ is the target operation wavelength) with different central bridge widths (6, 12, 24, 48, 96, and 192 nm). Since small changes in the nanocavity geometry may have a high impact on the Purcell factor, optimizations are carried out using identical discretization parameters to obtain directly comparable results. Through this systematic study, we achieve insight about the limits on Purcell enhancement and the relationship between Q and V for optimized designs for different geometric constraints.

2. Methods

The design and optimization of nanobeam cavities with large Purcell factors for single emitters are formulated as a frequency domain scattering problem with the goal of magnifying the local density of states (LDOS) as proposed by Liang and Johnson [35]. The Purcell factor is the

ratio of the LDOS at the position \mathbf{r} relative to the LDOS in a homogeneous medium of the same refractive index. The physics of the photonic nanobeam cavity problem is modeled in the 3D domain Ω (Fig. 2(a)) by Maxwell's equations under a steady-state assumption. The wave equation governing the electric field in the domain may be written as,

$$\nabla \times \frac{1}{\mu_r(\mathbf{r})} \nabla \times \mathbf{E}(\omega, \mathbf{r}) - \frac{\omega^2}{c^2} \epsilon_r(\mathbf{r}) \mathbf{E}(\omega, \mathbf{r}) = i\omega\mu_0 \mathbf{J}(\omega, \mathbf{r}), \quad \mathbf{r} \in \Omega \in \mathcal{R}^3, \quad (1)$$

where \mathbf{E} denotes the electric field, ω is the free-space angular frequency, $\mu_r(\mathbf{r})$ is the relative permeability, $\epsilon_r(\mathbf{r})$ is the relative permittivity, i denotes the imaginary unit, μ_0 is the free-space permeability and $\mathbf{J} = -i\omega \mathbf{p} \delta(\mathbf{r} - \mathbf{r}_c)$ is the current density with dipole moment \mathbf{p} that defines an electric dipole excitation source placed at the center of the cavity (\mathbf{r}_c). Finite element analysis [36] is used to solve the model problem. Top-view and side-view schematics of the model problem are depicted in Fig. 2(b), where the parameters related to dimensions are recorded in Table 1. In order to reduce the computational cost associated with solving the model problem, 3-fold mirror symmetry is imposed, allowing only one-eighth of the physical domain to be modeled by applying perfect electric conductor (PEC) and perfect magnetic conductor (PMC) boundary conditions as shown from Fig. 2(b) to 2(c). First-order absorbing boundary conditions (ABS) are used for truncating the domain.

Table 1. Dimensions for nanobeam cavity given in Fig. 2(b) for different design widths and target wavelength $\lambda = 1550$ nm

Cavity Design	w_{model}	d_{model}	h_{model}	w_{design}	d_{design}	h_{design}
Widths	[nm]	[nm]	[nm]	[nm]	[nm]	[nm]
4λ	6820	3800	3350	6200	700	250
2λ	3410	3800	3350	3100	700	250
1λ	1860	3800	3350	1550	700	250

The electric dipole source, oriented along y and located at the position \mathbf{r}_c in the center of the bridge domain (red region in Fig. 2(a)), is indicated with a green dot in the reduced computational domain in Fig. 2(c). The LDOS is calculated using [37],

$$LDOS(\omega, \mathbf{r}') = \frac{12\epsilon_0\epsilon_r(\mathbf{r})}{\pi\omega^2|\mathbf{p}|^2} P(\omega, \mathbf{r}') = -\frac{6\epsilon_0\epsilon_r(\mathbf{r}')}{\pi\omega^2|\mathbf{p}|^2} \text{Re} \left[\int \mathbf{J}^*(\omega, \mathbf{r}) \cdot \mathbf{E}(\omega, \mathbf{r}) d\mathbf{r} \right], \quad (2)$$

Here $P(\omega, \mathbf{r}')$ is power radiated by the dipole at position \mathbf{r}' which is targeted in the optimization to maximize LDOS. A design field $\xi(\mathbf{r}) \in [0, 1]$ is defined to control the material distribution by using the following interpolation scheme [38],

$$\epsilon_r(\xi(\mathbf{r})) = \epsilon_{r,air} + \xi(\mathbf{r}) (\epsilon_{r,si} - \epsilon_{r,air}), \quad \mathbf{r} \in \Omega, \quad (3)$$

where $\epsilon_{r,air}$ is the relative permittivity of air ($\epsilon_{r,air} = 1.0$) and $\epsilon_{r,si}$ is the relative permittivity of the silicon ($\epsilon_{r,si} = 12.1104$). The design field is kept constant in the out-of-plane (z) direction to impose material invariance, which ensures that the designs are realizable using electron-beam lithography or similar fabrication techniques. A well-known filtering and thresholding approach is applied to the design field [39,40]. The optimization problem is solved using the globally convergent method of moving asymptotes (GCMMA) [41]. The sensitivities with respect to the design variables are computed by adjoint sensitivity analysis [42].

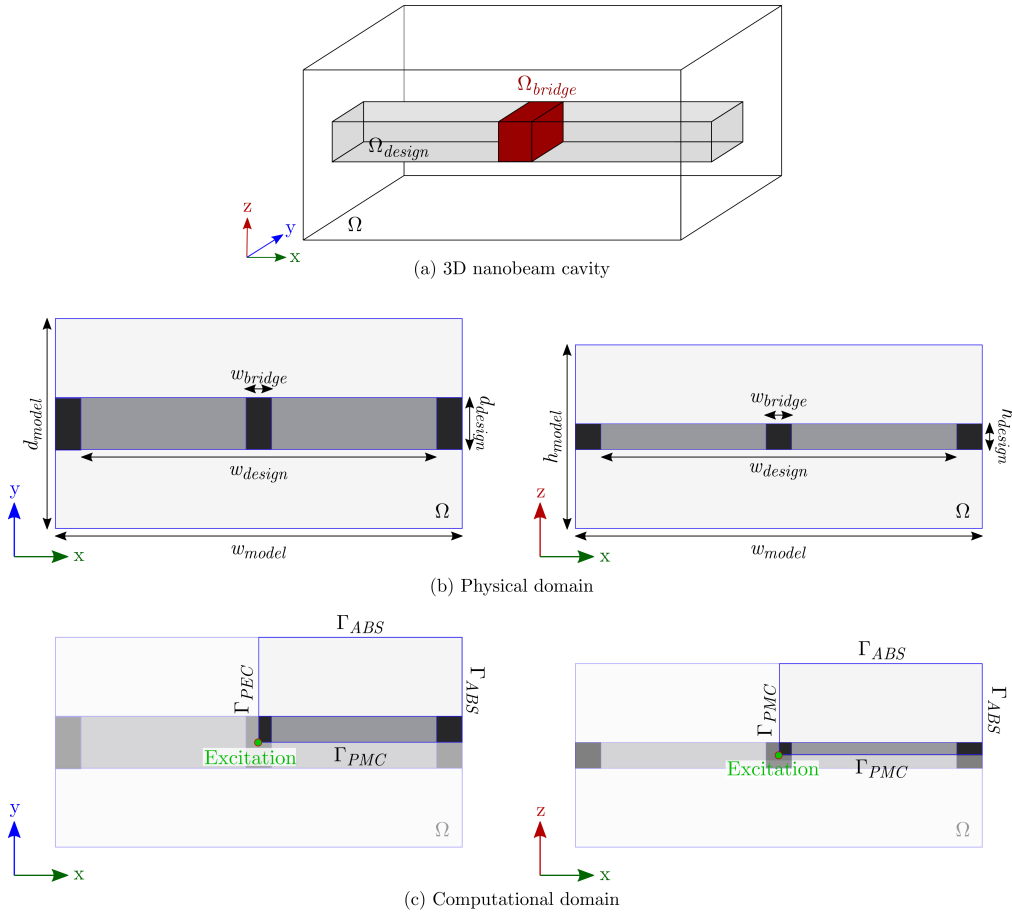


Fig. 2. Visualization of 3D nanobeam cavity model for both physical and computational domains: (a) 3D view of nanobeam cavity domain (Ω); bridge region is shown with red color (Ω_{bridge}) positioned in the middle of the designable part of the nanobeam (Ω_{design}). (b) Top (left) and side (right) view of the physical domain, fixed part filled with silicon of the nanobeam depicted with black color, i.e., bridge part and coupled waveguides termination at both sides of the domain. Design domain represented with dark gray color and air region surrounding nanobeam shown with light gray color. (c) Top (left) and side (right) view of the reduced computational domain (one-eighth of the physical domain) with the dipole excitation and corresponding boundary conditions.

After obtaining the optimized designs, the resonant mode of the nanobeam cavity can be found by solving the following eigenvalue problem,

$$\nabla \times \frac{1}{\mu_r(\mathbf{r})} \nabla \times \mathbf{E}_n(\mathbf{r}) - \frac{\omega_n^2}{c^2} \epsilon_r(\mathbf{r}) \mathbf{E}_n(\mathbf{r}) = 0, \quad (4)$$

where ω_n represents the eigenfrequency of n^{th} mode. The quality factor and mode volume for the mode corresponds to frequency ω_n can be found as

$$Q = -\frac{\text{Re}[\omega_n]}{2\text{Im}[\omega_n]}, \quad (5)$$

$$v = \frac{\lim_{\mathcal{V} \rightarrow \infty} \int_{\mathcal{V}} \epsilon_r(\mathbf{r}) \mathbf{E}_n(\mathbf{r}) \cdot \mathbf{E}_n(\mathbf{r}) d\mathbf{r} + i \frac{c \sqrt{\epsilon_{r,\text{air}}}}{2\omega_n} \int_{\partial\mathcal{V}} \mathbf{E}_n(\mathbf{r}) \cdot \mathbf{E}_n(\mathbf{r}) d\mathbf{r}}{\epsilon_r(\mathbf{r}_c) \mathbf{E}_n(\mathbf{r}_c) \cdot \mathbf{E}_n(\mathbf{r})}, \quad (6)$$

$$V = \frac{1}{\text{Re}[1/v]}. \quad (7)$$

where $\partial\mathcal{V}$ is the boundary of the volume \mathcal{V} , the \mathbf{r}_c corresponds to the center of the nanobeam cavity (i.e., the center of the bridge region). In practice, the integral is taken over the volume of the calculation domain. The surface term in Eq. (6) acts then as an effective regularization of the otherwise divergent volume integral [43,44]. In the limit of infinite quality factor - for which the fields do not extend outside the cavity region - the general formulation in Eq. (6) recovers the

familiar expression $V = \frac{\int_{\mathcal{V}} \epsilon_r(\mathbf{r}) |\mathbf{E}_n(\mathbf{r})|^2 d\mathbf{r}}{\epsilon_r(\mathbf{r}_c) |\mathbf{E}_n(\mathbf{r}_c)|^2}$. In this work, we have found that even at the finite Q -values we consider in this work the two expressions yields near identical results.

The optimization and eigenvalue problems are discretized and solved using COMSOL Multiphysics 5.6 [45] on high performance computing clusters provided by DTU Computing Center [46]. The inverse design procedure has been implemented following the description in Christiansen et al. [47] with appropriate modifications. Very fine finite element meshes are required to accommodate intricate geometry control and ensure sufficient numerical precision. It is noted that the numerical discretization can have a strong influence on the accuracy of the simulation, especially for highly resonant structures. Therefore, a mesh convergence study was conducted to ensure sufficient accuracy of the mesh on which the inverse design was performed. A hybrid mesh was employed by using a structured mesh of brick elements for the nanobeam, with a minimum of four elements used to resolve the central bridge feature, combined with a free mesh of tetrahedral elements for the surrounding region. Even when taking advantage of eight-fold symmetry, the finite element models involve up to 1 million elements (element sizes are 2 nm near the center), 2.5 million degrees of freedom, and computational times approach two weeks for the largest design domains. While process-specific fabrication constraints are not accounted for in this study, it is worth noting that it has recently been demonstrated that nanocavities designed using topology optimization, exhibit good agreement between numerical and experimental results, when explicitly incorporating fabrication specific constraints in the inverse design process [24]. Optimization results are also prone to local minima; hence all designs have been selected as the best designs for a handful of different starting guesses and cross-checked for consistency. Nevertheless, global minima cannot be guaranteed, but the consistency of the obtained designs gives faith in high quality of the results obtained.

3. Results and discussion

Our numerical experiments consider nanobeam cavity structures with different design domain widths and bridge widths. The target wavelength (λ) is selected as 1550 nm, and the design

domain widths for the nanobeam cavities are chosen as 1λ , 2λ , and 4λ . The widths of the fixed bridge region (w_b) located in the center are selected as 6, 12, 24, 48, 96, and 192 nm, respectively.

The optimized designs are presented in Fig. 3 organized by their bridge widths and design domain widths. In this figure, the bridge width increases from top to bottom, and the design domain size increases from left to right. The black regions correspond to silicon, and the light gray regions indicate air.

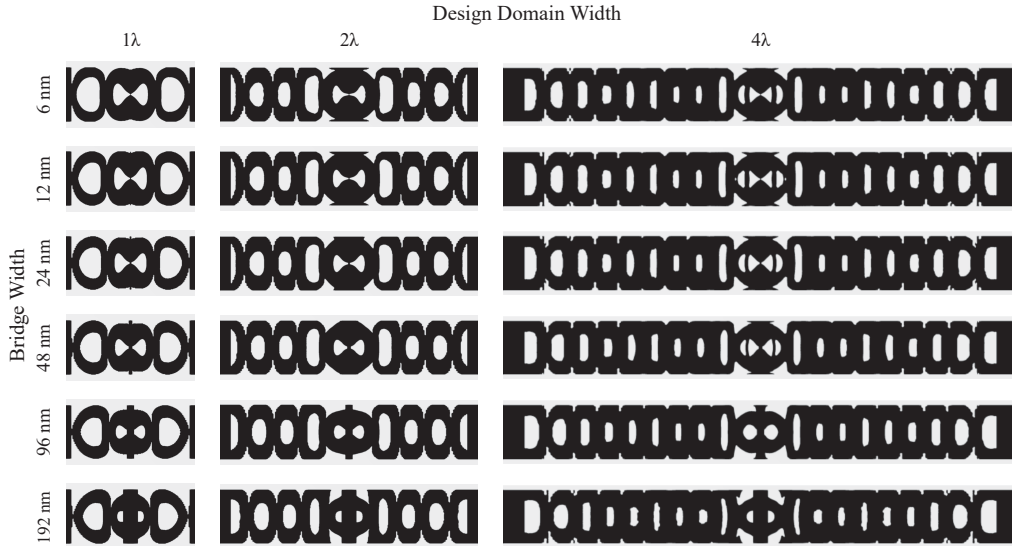


Fig. 3. Optimized nanocavity designs: design domain widths 1λ , 2λ , and 4λ from left to right; bridge widths 6, 12, 24, 48, 96, and 192 nm from top to bottom, respectively.

For the optimized designs illustrated in Fig. 3, the computed Q/V -ratio, quality factor, and mode volume as a function of bridge width and design domain width are reported on double-logarithmic plots in Figs. 4 and 5. In order to formulate the changes in the metrics as a function of bridge width, linear regression (with logarithmic inputs) is used in Fig. 4. It is shown that the spatial confinement depends strongly on bridge width. The Q/V -ratio mainly shows an inverse proportional relation to bridge width since the relative dependency of Q on the bridge width is weaker than the dependency of V . The highest Q/V -ratio found in this study was 3.66×10^4 ($2n_{si}/\lambda$)³ obtained for the 4λ sized nanobeam cavity with 6 nm bridge width. The quality factor is observed to consistently increase with bridge width, as the nanobeam with the largest design domain and 192 nm bridge width shows the largest Q value of 1.10×10^4 . Mode volume values below the diffraction limit are observed in 11 out of 18 nanobeam designs and are seen to drop with bridge-width size consistently. The lowest value, $V = 5.61 \times 10^{-2}$ ($\lambda/(2n_{si})$)³ is found for the nanobeam with the smallest design domain size (for $w_b = 6$ nm).

The findings of Figs. 3, 4, and 5 can be summarized as follows

- The highest Q/V -ratio design (i.e. the design facilitating the largest Purcell enhancement) does not have the highest Q or the lowest V in the data set, clearly showing a trade-off between the two metrics. The Q/V -ratio for a fixed sized nanobeam cavity drops as the bridge width gets larger. Similarly, the Q/V -ratio decreases proportionally to the design domain size for a given bridge width. In Fig. 5, one observes similar Purcell factors obtained by different designs. As an example, values of the metrics for two different nanobeam cavities with similar Q/V -ratios are shown in Table 2. The larger footprint design is seen to obtain its Q/V -ratio from supporting a larger quality factor at a larger V , while the smaller

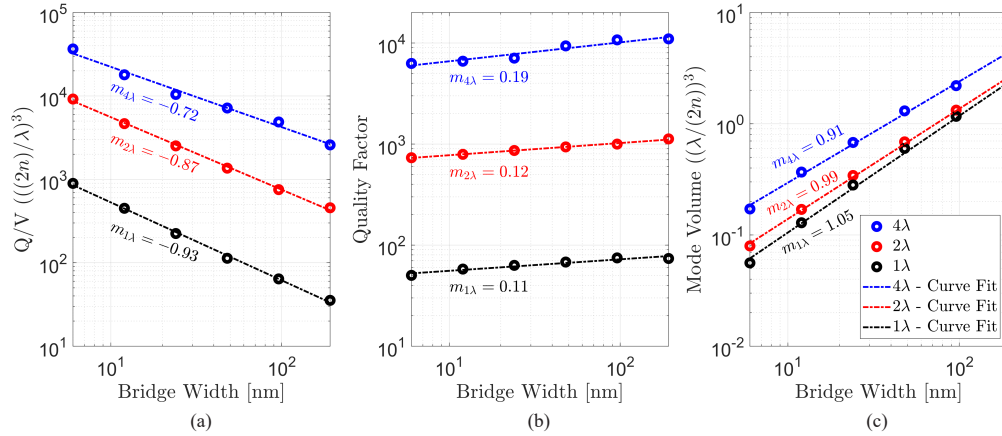


Fig. 4. (a) Q/V -ratio, (b) Q , and (c) V values as a function of bridge width for optimized nanobeam cavities with design domain sizes 4λ (blue), 2λ (red) and 1λ (black) are shown as circles. The curve fitted data (linear regression) for the metrics with respect to bridge width are depicted as dash-dot lines with the same color scheme and the slope of the curves are given by $m_{n\lambda}$.

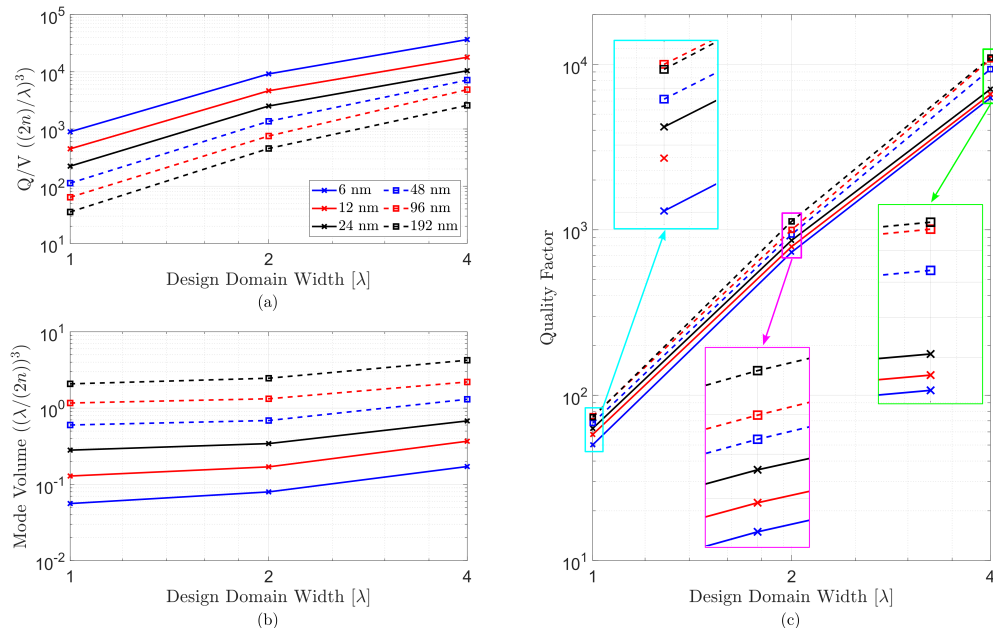


Fig. 5. (a) Q/V -ratio, (b) V and (c) Q values as a function of design domain width for optimized nanobeam cavities with bridge widths 6 nm (blue cross), 12 nm (red cross), 24 nm (black cross), 48 nm (blue square), 96 nm (red square), and 192 nm (black square) are illustrated. The zoom-in frames of Q values for different sizes 1λ (cyan frame), 2λ (magenta frame) and 4λ (green frame) are demonstrated.

footprint design achieves its similar Q/V -ratio by supporting a significantly smaller mode volume at a lower Q -value.

- In nearly all cases we observe that the quality factor increases when the bridge width increases. The only exception is the smallest nanobeam cavity with $w_b = 196$ nm. The smaller design freedom for the smallest cavity might be the main reason for this dependence on Q , since the given design domain widths already include the bridge width. Nevertheless, a significant drop in the Q values can be observed for decreasing beam size (due to smaller design domain sizes), which agrees with the previous literature [26,27]; demonstrating the need for a larger footprint to achieve higher Q values as recorded by Asano et al. [23].
- The mode volume is observed to consistently decrease with decreasing cavity size for all choices of the bridge width. This can be attributed to the upper limit on the achievable quality factor dictated by the cavity size. In turn, limited Q forces the optimization algorithm to exploit a smaller V in order to maximize the Purcell enhancement. Furthermore, the mode volume is seen to scale linearly with bridge width.
- Nearly all designs exhibit a central bowtie-like feature. When the bridge width increases, the air holes get smaller, and the sharp edges in the bowties fade into rounded holes. Since a tight spatial confinement becomes increasingly difficult with larger bridge widths, this change in the shape of the central air holes increases the Q values. Periodic nanoholes surround these bowtie regions close to the bridge, which serve to increase the quality factor.

Table 2. Comparison of metrics for two optimized designs with similar Q/V -ratios while having different geometric limitations.

Cavity Design	w_{bridge}	Q/V -ratio	Q	V
Widths	[nm]	$(2n_{sl}/\lambda)^3$		$(\lambda/(2n_{sl}))^3$
4λ	192	2.59×10^3	1.10×10^4	4.25
2λ	24	2.52×10^3	8.63×10^2	3.43×10^{-1}

The results consistently demonstrate a trade-off between temporal and spatial confinement. The largest Purcell factor is not achieved for the design with the highest Q nor the design with the lowest V ; instead, it is found in a design exploiting a trade-off between these two metrics. This trade-off can also be observed when comparing the designs of Asano [23] and Choi [19] for large Purcell factor, with the former focused on maximizing Q and the latter on minimizing V . In contrast, in this study, neither Q nor V is individually targeted; instead, inverse design by topology optimization is exploited to directly target maximization of the Purcell factor, allowing the best possible trade-off between Q and V to be identified. Utilizing topology optimization as a robust inverse design tool, we thus explored the relationship between spatial and temporal confinement for maximizing Purcell enhancement more systematically than allowed by intuition-based design. Previous works [23,27] have shown that larger Q/V -ratios can be achieved by significantly larger device footprints, allowing much higher quality factors than the devices designed and studied in this work. However, such large footprint devices are impractical for many applications. Hence, we limit our study to cavities with relatively small footprints to explore the limits on Q/V -ratio.

4. Conclusion

A systematic study of the effect of geometric constraints in photonic structures on the achievable Purcell factor enhancement for a single emitter was presented. The optimized designs were analyzed in terms of their temporal (Q) and spatial (V) confinement of the optical field. We

find that a trade-off between Q and V is required in order to maximize the Purcell enhancement. That is, a given design does not simultaneously achieve the highest Q and lowest V in order to maximize the Purcell enhancement. It was found that V mainly scales near linearly with the allowed length-scale (bridge width) near the emitter position, while the quality factor mainly scales with overall device size.

Funding. Danmarks Grundforskningsfond (DNRF147).

Disclosures. The authors declare no conflicts of interest.

Data Availability. A device blueprint of the nanobeam cavity design with a 6 nm bridge width and one wavelength design domain size is supplied as an example, see [Dataset 1 \[48\]](#) for supporting content. The additional device blueprints are also available from the corresponding author upon request.

References

1. E. M. Purcell, "Spontaneous emission probabilities at radio frequencies," *Phys. Rev.* **69**(1-2), 37–38 (1946).
2. P. Goy, J. M. Raimond, M. Gross, and S. Haroche, "Observation of cavity-enhanced single-atom spontaneous emission," *Phys. Rev. Lett.* **50**(24), 1903–1906 (1983).
3. D. J. Heinzen, J. J. Childs, J. E. Thomas, and M. S. Feld, "Enhanced and inhibited visible spontaneous emission by atoms in a confocal resonator," *Phys. Rev. Lett.* **58**(13), 1320–1323 (1987).
4. J. M. Gérard, B. Sermage, B. Gayral, B. Legrand, E. Costard, and V. Thierry-Mieg, "Enhanced spontaneous emission by quantum boxes in a monolithic optical microcavity," *Phys. Rev. Lett.* **81**(5), 1110–1113 (1998).
5. P. Lodahl, A. Driel, I. Nikolaev, A. Irman, K. Overgaag, D. Vanmaekelbergh, and W. Vos, "Controlling the dynamics of spontaneous emission from quantum dots by photonic crystal," *Nature* **430**(7000), 654–657 (2004).
6. X. Ding, Y. He, Z.-C. Duan, N. Gregersen, M.-C. Chen, S. Unsleber, S. Maier, C. Schneider, M. Kamp, S. Höfling, C.-Y. Lu, and J.-W. Pan, "On-demand single photons with high extraction efficiency and near-unity indistinguishability from a resonantly driven quantum dot in a micropillar," *Phys. Rev. Lett.* **116**(2), 020401 (2016).
7. Y. Yamamoto, S. Machida, and G. Björk, "Microcavity semiconductor laser with enhanced spontaneous emission," *Phys. Rev. A* **44**(1), 657–668 (1991).
8. E. K. Lau, A. Lakhani, R. S. Tucker, and M. C. Wu, "Enhanced modulation bandwidth of nanocavity light emitting devices," *Opt. Express* **17**(10), 7790–7799 (2009).
9. T. Suhr, N. Gregersen, K. Yvind, and J. Mørk, "Modulation response of nanoleds and nanolasers exploiting purcell enhanced spontaneous emission," *Opt. Express* **18**(11), 11230–11241 (2010).
10. J. Mørk and G. L. Lippi, "Rate equation description of quantum noise in nanolasers with few emitters," *Appl. Phys. Lett.* **112**(14), 141103 (2018).
11. J. Khurgin, "How to deal with the loss in plasmonics and metamaterials," *Nat. Nanotechnol.* **10**(1), 2–6 (2015).
12. P. I. Borel, A. Harpøth, L. H. Frandsen, M. Kristensen, P. Shi, J. S. Jensen, and O. Sigmund, "Topology optimization and fabrication of photonic crystal structures," *Opt. Express* **12**(9), 1996 (2004).
13. J. S. Jensen and O. Sigmund, "Topology optimization for nano-photonics," *Laser Photonics Rev.* **5**(2), 308–321 (2011).
14. S. Molesky, Z. Lin, A. Y. Piggott, W. Jin, J. Vucković, and A. W. Rodriguez, "Inverse design in nanophotonics," *Nat. Photonics* **12**(11), 659–670 (2018).
15. M. P. Bendsoe and N. Kikuchi, "Generating optimal topologies in structural design using a homogenization method," *Comput. Methods Appl. Mech. Eng.* **71**(2), 197–224 (1988).
16. M. Bendsoe and O. Sigmund, *Topology Optimization - Theory, Methods, and Applications* (Springer Verlag, 2003).
17. F. Wang, R. E. Christiansen, Y. Yu, J. Mørk, and O. Sigmund, "Maximizing the quality factor to mode volume ratio for ultra-small photonic crystal cavities," *Appl. Phys. Lett.* **113**(24), 241101 (2018).
18. J. T. Robinson, C. Manolatu, L. Chen, and M. Lipson, "Ultrasmall mode volumes in dielectric optical microcavities," *Phys. Rev. Lett.* **95**(14), 143901 (2005).
19. H. Choi, M. Heuck, and D. Englund, "Self-Similar Nanocavity Design with Ultrasmall Mode Volume for Single-Photon Nonlinearities," *Phys. Rev. Lett.* **118**(22), 223605 (2017).
20. P. Velha, E. Picard, T. Charvolin, E. Hadji, J. Rodier, P. Lalanne, and D. Peyrade, "Ultra-High Q/V Fabry-Perot microcavity on SOI substrate," *Opt. Express* **15**(24), 16090 (2007).
21. P. Seidler, K. Lister, U. Drechsler, J. Hofrichter, and T. Stöferle, "Slotted photonic crystal nanobeam cavity with an ultrahigh quality factor-to-mode volume ratio," *Opt. Express* **21**(26), 32468 (2013).
22. S. Hu and S. M. Weiss, "Design of photonic crystal cavities for extreme light concentration," *ACS Photonics* **3**(9), 1647–1653 (2016).
23. T. Asano, Y. Ochi, Y. Takahashi, K. Kishimoto, and S. Noda, "Photonic crystal nanocavity with a Q factor exceeding eleven million," *Opt. Express* **25**(3), 1769 (2017).
24. M. Albrechtsen, B. Lahijani, R. Christiansen, V. Nguyen, L. Casses, S. Hansen, N. Stenger, O. Sigmund, H. Jansen, J. Mørk, and S. Stobbe, "Nanometer-scale photon confinement in topology-optimized dielectric cavities," *Nat. Commun.* **13**(1), 6281 (2022).
25. M. Albrechtsen, B. V. Lahijani, and S. Stobbe, "Two regimes of confinement in photonic nanocavities: bulk confinement versus lightning rods," *Opt. Express* **30**(9), 15458–15469 (2022).

26. D. W. Vernooy, V. S. Ilchenko, H. Mabuchi, E. W. Streed, and H. J. Kimble, "High-q measurements of fused-silica microspheres in the near infrared," *Opt. Lett.* **23**(4), 247–249 (1998).
27. Y. Akahane, T. Asano, B. S. Song, and S. Noda, "High-Q photonic nanocavity in a two-dimensional photonic crystal," *Nature* **425**(6961), 944–947 (2003).
28. Q. Zhao, L. Zhang, and O. D. Miller, "Minimum dielectric-resonator mode volumes," *arXiv*, arXiv:2008.13241 (2020).
29. M. K. Schmidt, C. G. Poulton, and M. J. Steel, "Acoustic diamond resonators with ultrasmall mode volumes," *Phys. Rev. Res.* **2**(3), 033153 (2020).
30. H. Choi, D. Zhu, Y. Yoon, and D. Englund, "Cascaded Cavities Boost the Indistinguishability of Imperfect Quantum Emitters," *Phys. Rev. Lett.* **122**(18), 183602 (2019).
31. J. G. Bartholomew, J. Rochman, T. Xie, J. M. Kindem, A. Ruskuc, I. Craiciu, M. Lei, and A. Faraon, "On-chip coherent microwave-to-optical transduction mediated by ytterbium in YVO₄," *Nat. Commun.* **11**(1), 3266 (2020).
32. M. Heuck, K. Jacobs, and D. R. Englund, "Photon-photon interactions in dynamically coupled cavities," *Phys. Rev. A* **101**(4), 042322 (2020).
33. H. Choi, L. Ateshian, M. Heuck, and D. Englund, "Terahertz Light Sources by Electronic-Oscillator-Driven Second-Harmonic Generation in Cavities Featuring Extreme Confinement," *Phys. Rev. Appl.* **18**(4), 044019 (2022).
34. A. M. Hammond, A. Oskooi, S. G. Johnson, and S. E. Ralph, "Photonic topology optimization with semiconductor-foundry design-rule constraints," *Opt. Express* **29**(15), 23916 (2021).
35. X. Liang and S. G. Johnson, "Formulation for scalable optimization of microcavities via the frequency-averaged local density of states," *Opt. Express* **21**(25), 30812 (2013).
36. J.-M. Jin, *The Finite Element Method in Electromagnetics* (Wiley-IEEE Press, 2014).
37. L. Novotny and B. Hecht, *Principles of Nano-Optics* (Cambridge University Press, 2012), 2nd ed.
38. R. E. Christiansen, J. Vester-Petersen, S. P. Madsen, and O. Sigmund, "A non-linear material interpolation for design of metallic nano-particles using topology optimization," *Comput. Methods Appl. Mech. Eng.* **343**, 23–39 (2019).
39. J. K. Guest, J. H. Prévost, and T. Belytschko, "Achieving minimum length scale in topology optimization using nodal design variables and projection functions," *Int. J. Numer. Meth. Engng.* **61**(2), 238–254 (2004).
40. F. Wang, B. S. Lazarov, and O. Sigmund, "On projection methods, convergence and robust formulations in topology optimization," *Struct. Multidiscip. Optim.* **43**(6), 767–784 (2011).
41. K. Svanberg, "A Class of Globally Convergent Optimization Methods Based on Conservative Convex Separable Approximations," *SIAM J. Optim.* **12**(2), 555–573 (2002).
42. D. Tortorelli and P. Michaleris, "Design sensitivity analysis: Overview and review," *Inverse Probl. Eng.* **1**(1), 71–105 (1994).
43. P. T. Kristensen, C. Van Vlack, and S. Hughes, "Effective mode volumes for leaky optical cavities," *AIP Conf. Proc.* **1398**, 100–102 (2011).
44. P. T. Kristensen, R.-C. Ge, and S. Hughes, "Normalization of quasinormal modes in leaky optical cavities and plasmonic resonators," *Phys. Rev. A* **92**(5), 053810 (2015).
45. S. COMSOL AB, Stockholm, "Comsol multiphysics v. 5.6," (2022).
46. DTU Computing Center, "DTU Computing Center resources," (2022).
47. R. E. Christiansen and O. Sigmund, "Inverse design in photonics by topology optimization : tutorial," *J. Opt. Soc. Am. B* **38**(2), 496–509 (2021).
48. G. Işıklar, "A device blueprint of the nanobeam cavity design," figshare (2022), <https://doi.org/10.6084/m9.figshare.21498600>.